6th Australasian Hydraulics and
Fluid Mechanics Conference
Adelaide, Australia, 5-9 December 1977

# Field Measurements of the Characteristics of a Rural Boundary Layer Near the Ground: Part I — The Measured Data

D. LINDLEY

Senior Lecturer, Department of Mechanical Engineering, University of Canterbury, N.Z.

R. FLAY

Graduate Student, Department of Mechanical Engineering, University of Canterbury, N.Z.

and

A. J. BOWEN

Senior Lecturer, Department of Mechanical Engineering, University of Canterbury, N.Z.

SUMMARY Results of field measurements of the characteristics of a rural boundary layer within 19 m of the ground are presented. The experiment represents an attempt to obtain a comprehensive set of data from a single site. The results compare well with other available measured data.

## 1 INTRODUCTION

A system has been developed for the measurement of the characteristics of the atmospheric boundary layer near the ground. It is based on the use of orthogonal arrays of 4-bladed, 19.05 cm diameter polystyrene propeller anemometers. Each propeller drives a shaft mounted disc containing 32 slots. The disc rotates between two light emitting diodes and photo-receivers. Both these photo receivers produce a square-wave and their relative positions are such that the two square-waves are $90^{o}$ out of phase. From this, the direction of rotation can be decoded. One square-wave from the anemometer drives an 8-bit counter, 1 bit from this counter being used to give direction of rotation and the other 7 bits to give the rotational speed.

The counters are allowed to count for a selected period of time, after which their contents are written on to 7-track magnetic tape in the form of 512 six-bit words. The data tape is later processed on a Burroughs 6700 computer. Altogether, 36 anemometers in 12 orthogonal arrays mounted on a series of towers, the highest of which will allow measurements up to 25 metres, are to be used in a range of field measurements. Earlier work on the determination of the characteristics of these and other sensors has already been reported. (Lindley, Bowen and Morfee, 1974; Lindley and Bowen, 1974 and Lindley, 1975.)

The measurement system is to be used in experiments to determine:-

i) the variation of velocity, energy and turbulence over escarpments;
ii) the flow field upstream and downstream of an operational 4.7 m diameter Darrieus windmill;
iii) the characteristics of a rural boundary layer as they affect the design of electrical transmission lines and towers;
iv) wind structure characteristics as they affect the design and operation of large (up to 70 m diameter) windmills.

Much of the field work completed to date has been concerned with (i) above, and has relied upon the use of cup anemometers as wind speed sensors. This earlier data and comparisons with wind tunnel experiments and a finite element frozen vorticity analysis has already been reported. (Bowen and Lindley, 1974; 1977; and Lindley, Astley, Flay and Bowen, 1977.)

More detailed measurements of wind structure are now required and as part of a calibration procedure for the propeller anemometer system, experiments have been conducted in a rural boundary layer. These measurements are to be compared with well-established data for similar terrain where they exist. This paper presents some preliminary results of this work.

## 2 THE SITE

The major site features and dimensions are represented in Figure 1. It is situated on a research farm at Lincoln Agricultural College about 16 km south-west of Christchurch in the South Island of New Zealand. To the north of the site lies many kilometres of uninterrupted level plains of short grass with occasional trees, sparsely distributed shelter belts and farm buildings. As shown in the figure, a 5 to 6 m high shelter belt of fir trees lies 52 m to the south of the instrumented mast.

For the experiment 6 orthogonal arrays of propeller anemometers were mounted at 3.2, 5.2, 7.69, 10.2, 12.6, and 18.9 m above ground level. They were mounted on arms such that the arrays were 1 m from the tower which was itself a telescopic open lattice structure. The side of the triangular section tower varied from 0.3 m at the base to 0.05 m at the uppermost (pipe) section. The arrays were mounted with an open aspect to the northerly quarter. They were thus in the lee of the tower for southerly winds but completely open for all winds from the northerly quarter. The anemometers were hard wired to a data logger housed in a caravan some 100 m from the base of the mast.

## 3 MEAN WIND SPEED VARIATION WITH HEIGHT

The mean wind speed profile with height is given in Figure 2. Two sets of data have been used. One set was taken during a storm with an average velocity at 10 m of 12 m/s and a southerly direction so that it was passing through and over the shelter belt shown in the figure. The other data was for a wind with an average speed at 10 m of 4.5 m/s from the northerly direction. In both cases data points have been plotted by averaging lengths of the record; 4.5 and 9.1 minutes for the southerly direction and 4.5 and 36 minutes for the northerly wind.

The data is compared with the logarithmic profile given by $\bar{V} = \sqrt{-\overline{uw}}\, K \ln (\frac{z}{z_o})$ where $z_o$ has been taken to be $6 \times 10^{-2}$m, and K is the von Kármán constant. The profile given by $\frac{V}{V_h} = k(\frac{z}{z_h})^{\alpha}$

where $\alpha = 0.19$ is virtually coincident with the logarithmic profile.

The wind from the northerly, uninterrupted fetch can be seen to have a mean wind speed variation with height typical of that found by others for a rural boundary layer (Teunissen, 1970).

The data for the wind from the south has been clearly influenced by the presence of the shelter belt (which was approximately 6 m high). Mean velocities are substantially lower within 1.5 shelter belt heights off the ground. Beyond this they approach the rural boundary layer profile. It can be seen that for results presented here, the averaging time has had little effect.

## 4 TURBULENCE INTENSITY VARIATION WITH HEIGHT

The points plotted in Figure 3 have been derived from the same data stream for the northerly wind where $\bar{V}_{10} = 4.5$ m/s [wind speed profile plotted in Figure 2]. Longitudinal ($\sigma_u/\bar{V}_{\tilde{z}}$), lateral ($\sigma_v/\bar{V}_{\tilde{z}}$) and vertical ($\sigma_w/\bar{V}_{\tilde{z}}$) components have been derived from 36.4 minutes of data and have been left uncorrected for non-cosine response of the propellers. The same quantities have also been derived from 4.5 minutes of the same data stream to show the effect of correcting for non-cosine response of the anemometer. For comparison, values taken from ESDU (1974) for roughness lengths of $6\times10^{-2}$m and $2.5\times10^{-2}$m are shown. The measured data for $\sigma_u/\bar{V}_{\tilde{z}}$ is generally in good agreement with ESDU for $z_o = 2.5\times10^{-2}$m but yields lower values for $\sigma_v/\bar{V}_{\tilde{z}}$ and $\sigma_w/\bar{V}_{\tilde{z}}$. The site, which is on level grass plains with isolated trees has a value of $z_o$ (according to ESDU) of about $2.5\times10^{-2}$m. It is not surprising that the agreement for all components is not good, as the present data was for a wind with an average speed of 4.5 m/s at 10 m. In contrast ESDU data strictly applies to strong winds, defined as a wind for which the mean value averaged over one hour is greater than about 10 m/s at 10 m. ESDU data only applies strictly to heights greater than 5 m.

In Figure 4 turbulence data has been plotted for the southerly wind passing over the shelter belt [same data used in Figure 2]. The effect of the shelter belt at heights less than 13 m can be seen. At a height of 13 m and above the values of $\sigma_u/\bar{V}_{\tilde{z}}$, $\sigma_v/\bar{V}_{\tilde{z}}$ and $\sigma_w/\bar{V}_{\tilde{z}}$ correspond reasonably well with those for the northerly wind direction. There is fair agreement with ESDU data for $z_o = 6\times10^{-2}$m, a higher value having been selected in recognition of the shelter belt. Values of all components are considerably increased by the presence of the upwind shelter belt at heights below 13 m.

## 5 REYNOLDS STRESS COEFFICIENT

Values for $\overline{uw}/\sigma_u\sigma_w$ are plotted in Figure 5 and are seen to vary considerably with height in contrast to values taken from ESDU (1974). Of all the measurements this is probably the most difficult to make in the field. Small errors in setting up the vertical anemometer to measure the vertical velocity component can have a marked effect on the result. Much of the variability in the data is probably the result of small angular variations between the axes of the vertical anemometers and the vertical. (Though these were set up with great care using a theodolite.) At the early stage of this experiment only data for short averaging times has been processed and both these factors will subsequently be rectified in an attempt to obtain more credible data.

## 6 POWER SPECTRAL DENSITY

Power spectral density functions are plotted in Figures 6, 7 and 8 for the longitudinal (u), lateral (v) and vertical components (w) respectively. The spectra for $\bar{V} = 5$ m/s for a wind from a northerly direction in all three figures have been derived from a data stream of 16384 points collected at a recording frequency of 7.5 $H_z$ for a record length of 36.4 minutes.

In addition, in Figures 6 and 8 the spread of measured data from 'various sources', as recorded by ESDU (1974), is plotted for comparison.

Another more complete set of data for a stronger wind from the southerly direction has been represented by points representing the upper and lower bounds of the measured spectra. This set of data was from orthogonal arrays at heights of 3.2, 5.2, 7.69, 10.2, 12.6 and 18.9 m where the mean velocities for the 9.1 minute record were 5.8, 7.4, 9.9, 11.3, 12.5 and 12.4 m/s respectively.

Finally, a solid curve is drawn on each figure representing the spectral equation for the component so that:

for the u component

$$\frac{n\,Suu(n)}{\sigma_u^2} = \frac{4\,\tilde{n}_u}{(1 + 70.8\,\tilde{n}_u^2)^{5/6}}$$

for the v component

$$\frac{n\,Svv(n)}{\sigma_v^2} = \frac{4\tilde{n}_v(1 + 755.2\,\tilde{n}_v^2)}{(1 + 283.2\,\tilde{n}_v^2)^{11/6}}$$

for the w component

$$\frac{n\,Sww(n)}{\sigma_w^2} = \frac{4\tilde{n}_w(1 + 755.2\,\tilde{n}_w^2)}{(1 + 283.2\,\tilde{n}_w^2)^{11/6}}$$

where

$\tilde{n}_u = {}^xL_u n/\bar{V}_{\tilde{z}}$; $\tilde{n}_v = {}^xL_v n/\bar{V}_{\tilde{z}}$; $\tilde{n}_w = {}^xL_w n/\bar{V}_{\tilde{z}}$

and $z_o = 6\times10^{-2}$m; $z = 18.9$ m; $\bar{V}_{\tilde{z}} = 5$ m/s.

The present field data shows moderately good agreement with the ESDU data and the spectral equations. The agreement is less good at the low frequencies but this is improved when a trend removal process is used on the raw data. More will be said of this in Part II of this paper. The poorer agreement at the higher frequencies is explained by the limitations of the speed sensor which has a distance constant of approximately 0.9 m. Data above about 0.2 $H_z$ would require a correction for the frequency limitations of the instrument which has not been made in this case. (Horst, 1973).

## 7 AUTOCORRELATION FUNCTION

Figures 9, 10 and 11 plot the autocorrelation functions for the longitudinal, lateral and vertical velocity components. The plots are derived from the same data stream of 16384 points with $\bar{V} = 5$ m/s with a record length of 36.4 minutes obtained by taking an inverse Fourier transform of the power spectra. Again, the more complete set of data for the stronger wind from the southerly direction has been represented by

a hatched area representing the spread of results from the arrays at 3.2, 5.2, 7.69, 10.2, 12.6 and 18.9 m with mean wind speeds as given in Section 6, the length scale showing a tendency to increase with height.

For comparison, the autocorrelation function obtained from ESDU (1975) for $z_o = 6 \times 10^{-2}$ m, $\tilde{z} = 18.9$ m, and $\bar{V}_{\tilde{z}} = 5$ m/s is given for each component.

For the u component at $\tilde{z} = 18.9$ m, $\bar{V}_{\tilde{z}} = 5$ m/s, the integral length scale ($^{x}L_u$) computed from this plot is approximately 140 m. ESDU (1975) for the same condition yields $^{x}L_u$ of 88 m. The equation $^{x}L_u = 11.04 \sqrt{\tilde{z}}$ from Teunissen (1970) yields $^{x}L_u = 48$ m.

For the stronger wind (represented by the shaded area) $^{x}L_u$ is approximately 100 m at $\tilde{z} = 7.69$ m and $\bar{V}_{\tilde{z}} = 9.9$ m/s.

It is evident from these figures that the autocorrelation function does not fall away as quickly as is predicted using the ESDU (1975) formulations.

Again it must be said that the present field data is compromised in that in the one case it was derived from a record with mean wind speed for the whole record of only 5 m/s and where the mean speed fell away slowly over the recording period. In the other case the data has been processed for only 9.1 minutes.

Neither set of data has had any trend removal process applied and it is evident (see Part II) that this has to be done in cases when the mean wind speed varies because an assumption made when processing the data is that the recording is stationary.

## 8 CONCLUSIONS

The results, it is stressed, are preliminary. They have served to indicate to the authors (at least) that with proper attention to data processing techniques, and careful choice of wind conditions, that the system is capable of producing reliable data for the experiments intended and described briefly in Section 1.

## 9 REFERENCES


BOWEN, A.J., and LINDLEY, D. (1974). Measurements of the mean wind flow over various escarpment shapes. Proc. of the Fifth Australasian Conf.on Hydraulics and Fluid Mechanics, Christchurch, New Zealand, 1974. Vol.1, pp 211-19.

BOWEN, A.J., and LINDLEY, D. (1977). A wind tunnel investigation of the wind speed and turbulence characteristics close to the ground over various escarpment shapes. To be published in Journ. of Boundary Layer Meteorology.

ESDU 72026 (1972). Characteristics of wind speed in the lower layers of the atmosphere near the ground: Strong winds (neutral atmosphere). Engineering Sciences Data Unit, London, 1972.

ESDU 74031 (1974). Characteristics of atmospheric turbulence near the ground. Part II: Single point data for strong winds (neutral atmosphere). Ibid.

ESDU 75001 (1975). Characteristics of atmospheric turbulence near the ground. Part III: Variations in space and time for strong winds (neutral atmosphere). Ibid.

HORST, T.W. (1973). Corrections for response errors in a three-component propeller anemometer. Journ. of Applied Meteorology, Vol.12, June.

LINDLEY, D., BOWEN, A.J., and MORFEE, P. (1974) A propeller anemometer for a digital wind data acquisition system. Proc. of the Fifth Australasian Conf. on Hydraulics and Fluid Mechanics, Christchurch, New Zealand, 1974. Vol.1, pp 258-68.

LINDLEY, D., and BOWEN, A.J. (1974). The response of cup and propeller anemometers to fluctuating wind speeds. Ibid, Vol.1, pp 269-77.

LINDLEY, D. (1975). The design and performance of a 6-cup anemometer. Journ. of Applied Meteorology, Vol.14, No.6, pp 1135-45.

LINDLEY, D., ASTLEY, R.J., FLAY, R.G.J., and BOWEN, A.J. (1977). Topographical modification to the atmospheric boundary layer. Proc. of Conseil International du Batiment - 7th Congress and General Assembly. Edinburgh, September.

TEUNISSEN, H.W. (1970). Characteristics of the mean wind and turbulence in the planetary boundary layer. UTIAS Review No.32, October.


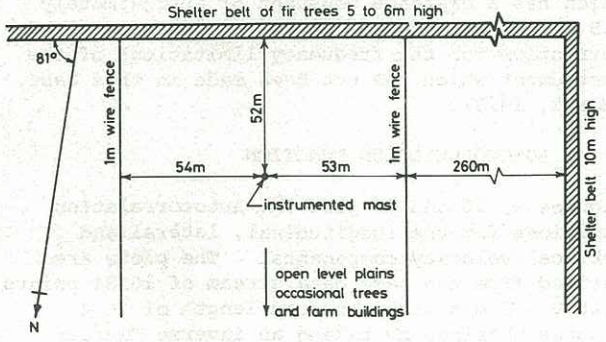


Figure 1 Measurement site.

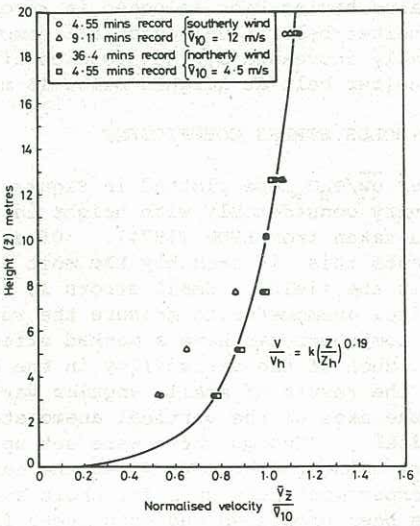


Figure 2 Normalised mean wind speed variation with height

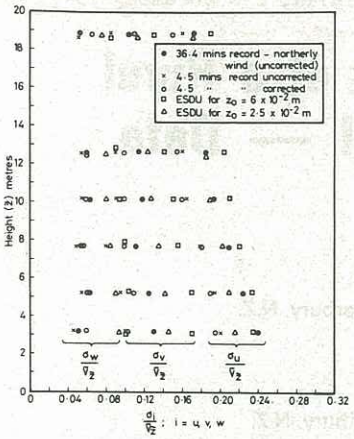


Figure 3 Turbulence intensity variation with height when $\bar{V}_{10}$ = 4.5 m/s.

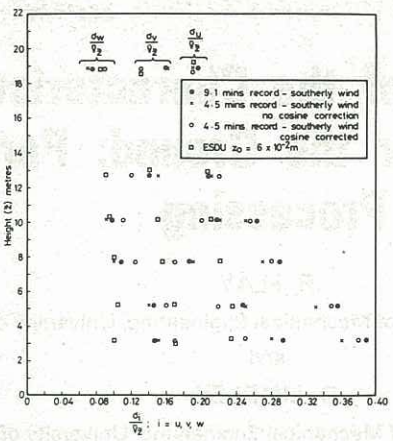


Figure 4 Turbulence intensity variation with height when $\bar{V}_{10}$ = 12 m/s.

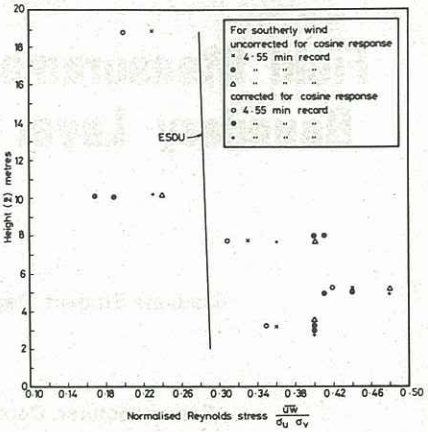


Figure 5 Reynolds stress variation with height when $\bar{V}_{10}$ = 12 m/s.

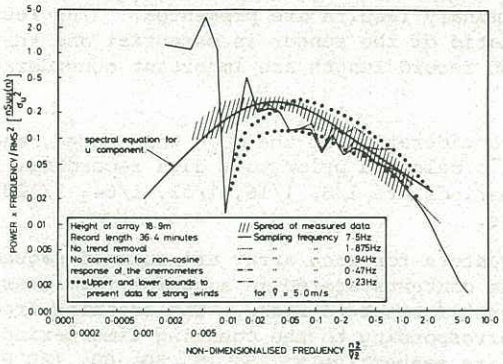


Figure 6 Power spectral density for the longitudinal component (u)

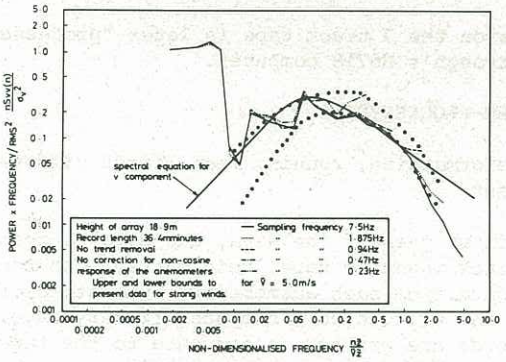


Figure 7 Power spectral density for the lateral component (v)

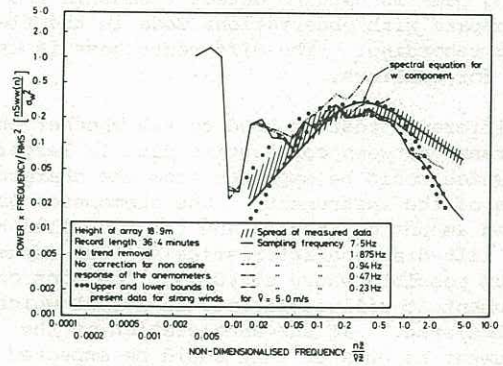


Figure 8 Power spectral density for the vertical component (w)

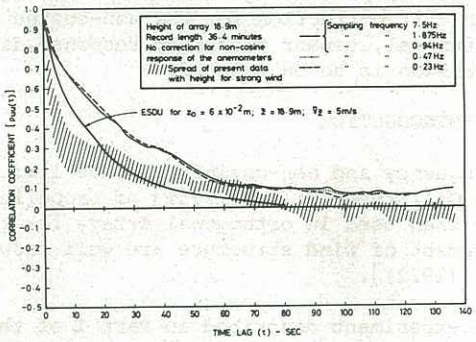


Figure 9 Autocorrelation function for the longitudinal velocity component (u)

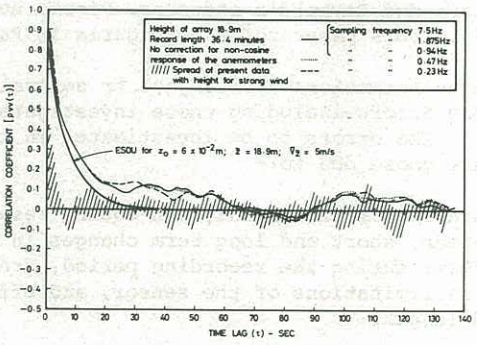


Figure 10 Autocorrelation function for the lateral velocity component (v)

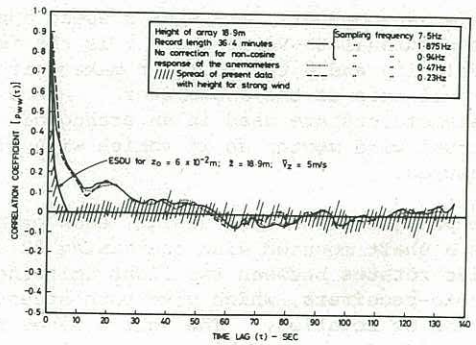


Figure 11 Autocorrelation function for the vertical velocity component (w)